3D Orientational Control in Self-Assembled Thin Films with Sub-5 nm Features by Light

*Koen Nickmans, Gerardus M. Bögels, Carlos Sánchez-Somolinos, Jeffrey N. Murphy, Philippe Leclère, Ilja K. Voets, and Albertus P. H. J. Schenning**

***While** self-assembled molecular building blocks could lead to many next-generation functional organic nanomaterials, control over the thin-film morphologies to yield monolithic sub-5 nm patterns with 3D orientational control at macroscopic length scales remains a grand challenge. A series of photoresponsive hybrid oligo(dimethylsiloxane) liquid crystals that form periodic cylindrical nanostructures with periodicities between 3.8 and 5.1 nm is studied. The liquid crystals can be aligned in-plane by exposure to actinic linearly polarized light and out-of-plane by exposure to actinic unpolarized light. The photoalignment is most efficient when performed just under the clearing point of the liquid crystal, at which the cylindrical nanostructures are reoriented within minutes. These results allow the generation of highly ordered sub-5 nm patterns in thin films at macroscopic length scales, with control over the orientation in a noncontact fashion.*

1. Introduction

Decades of soft matter research have yielded a plethora of building blocks, such as block copolymers (BCPs),[1–4] colloids,[5] surfactants,[6] and molecules,[7–9] which can self-assemble into a range of periodic nanostructures, such as lamellae, cylinders, or more complex geometries. Yet, the generation of defect-free thin-film nanostructure arrays remains a grand challenge due to the tendency of these building blocks to self-assemble into arbitrarily oriented poly-domain structures.[7] Nevertheless, achieving a thin-film monolithic alignment of these materials, across the molecule to device length scales,[10,11] could help to realize compelling advanced applications in areas such porous membranes,[12–14] organic electronics,[15] and nanolithography.[16–18]

While traditional BCPs have been the main driving force behind self-assembled thin-film applications,[1–4] sub-5 nm

K. Nickmans, Dr. G. M. Bögels, Dr. J. N. Murphy, Prof. A. P. H. J. Schenning
Laboratory of Functional Organic Materials and Devices
Department of Chemical Engineering and Chemistry
Eindhoven University of Technology
P.O. Box 513, 5600 MB, Eindhoven, The Netherlands
E-mail: a.p.h.j.Schenning@tue.nl

Dr. C. Sánchez-Somolinos
Departamento de Física de la Materia Condensada
Instituto de Ciencia de Materiales de Aragón (ICMA)
CSIC-Universidad de Zaragoza
50009 Zaragoza, Spain

Dr. Ph. Leclère
Laboratory for Chemistry of Novel Materials
Center for Innovation and Research in Materials and Polymers (CIRMAP)
University of Mons (UMONS)
Place du Parc 20, B 7000 Mons, Belgium

Dr. I. K. Voets, Prof. A. P. H. J. Schenning
Institute for Complex Molecular Systems
Eindhoven University of Technology
5600 MB, Eindhoven, The Netherlands

Dr. I. K. Voets
Laboratory of Macromolecular and Organic Chemistry
Department of Chemical Engineering and Chemistry
Eindhoven University of Technology
5600 MB, Eindhoven, The Netherlands

Dr. I. K. Voets
Laboratory of Physical Chemistry
Department of Chemical Engineering and Chemistry
Eindhoven University of Technology
5600 MB, Eindhoven, The Netherlands

DOI: 10.1002/smll.201701043

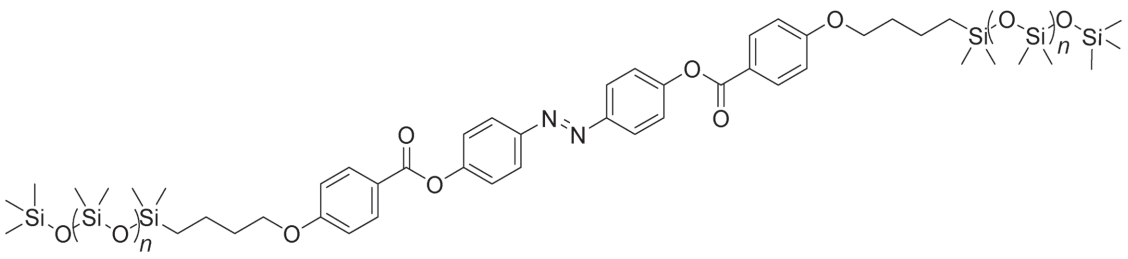

Scheme 1. Molecular structure of the ODMS liquid crystals, where *n* represents the length of the ODMS tail: LC-14Si (*n* = 5), LC-22Si (*n* = 9), and LC-30Si (*n* = 13).

periodicities are more readily formed by small molecules.[19,20] In bulk, these self-assembled small molecules have been aligned by, for example, shear,[21,22] alignment layers,[23,24] photoalignment,[25–31] magnetic fields,[14,32] and geometric confinement.[33–35] The induction of long-range order and orientational control in thin films is, however, a critical step toward the application of these small molecule nanomaterials as supramolecular templates.[7] In the sub-micrometer regime, photoalignment is a potentially well-suited method as it is noncontact, free of complex surface modification, and compatible with top–down microfabrication techniques.

Seki and Ikeda and their respective coworkers revealed that thin-film BCP morphologies consisting of amorphous phase segregated cylinders in an azobenzene (Az) liquid crystal (LC) matrix can be aligned with linearly polarized light (LPL).[36–42] The rod-like *trans* Azs are isomerized most effectively when their transition moments are oriented parallel to the electric vector (*E*) of light. In the case of normally incident LPL, this leads to a statistical buildup of Az moieties oriented orthogonal to *E*,[27,43–46] and the concurrent in-plane alignment of BCP nanostructures.[36–40] It was shown that the in-plane alignment of cylinders proceeds through subdomain rotation in a cooperative and synchronized manner.[47] In the case of normally incident unpolarized light, the Azs orient parallel to the light propagation direction minimizing their light absorption,[48] which allows the on-demand switching between in-plane and out-of-plane directions.

Recently, we reported a series of monodispersed organic–inorganic Az LCs containing oligo(dimethylsiloxane) (ODMS) for etch contrast that form sub-5 nm patterns,[49] and showed that their self-assembly can be directed in-plane by graphoepitaxy in a manner analogous to BCPs. Here, we demonstrate by a variety of techniques that the LC self-assembly can be directed both in-plane and out-of-plane with light, and that the mobility of the LC phase is key to achieving a rapid alignment. While it should be noted that photoalignment is a well-established method to align liquid crystals, both in terms of photoalignment layers[26,31,50] and the alignment of predominantly low-ordered nematic liquid crystals,[25,27,51] the 3D orientational control by light of ordered sub-5 nm periodicities in thin films has not been reported.

2. Results and Discussion

The molecular structure of the employed ODMS liquid crystals[49] is depicted in **Scheme 1**. The LCs consist of a photoresponsive *trans*-azobenzene containing rigid core flanked by flexible ODMS coils. Due to the bulkiness of the ODMS coils, the molecules form columnar liquid crystalline phases in which the LC cylinder is considered to be consisted of a stacked arrangement of rigid rods, while the matrix consists of ODMS. The phase behavior and associated lattice parameters are dependent on the length of the ODMS coil and temperature (**Table 1**). Dilute solutions of the Az liquid crystals with variant ODMS lengths displayed indistinguishable UV–vis absorption spectra (Figure S1, Supporting Information) with the characteristic π–π^* transition absorption band of the *trans* isomers with a peak at 330 nm and a weaker n–π^* transition absorption band with a maximum at 439 nm. The LCs isomerized from *trans* to *cis* upon irradiation with 365 nm UV light, resulting in a decreased absorbance at 330 nm, and an increase of the weaker n–π^* band at 439 nm indicating the formation of the *cis* isomer (Figure S2, Supporting Information). Subsequent irradiation with 455 nm light, at the low energy side of the n–π^* band, recovered the absorption spectra to the initial state consisting of predominantly *trans* isomers.

The photoresponsive properties the Az liquid crystals were first studied in thin untreated quartz cells (thickness ≈ 1.5 μm). **Figure 1** shows a schematic representation of the cylinder morphology, a polarized optical microscopy (POM) image, and polarized UV–vis spectroscopy data of LC-22Si in the cell. The observed birefringent texture under POM indicates that the optical axes of the domains (and also the columnar axes) are oriented randomly. Compared to its corresponding absorption in solution (Figure S3, Supporting Information), the π–π^* transition absorption peak exhibited some broadening, indicative of aggregated Az moieties in the LC state. However, no shift was observed, suggesting restricted Az aggregation in the LC state,[29] potentially as an effect of the bulky ODMS matrix. Polarized UV–vis absorption spectroscopy of the absorption at 330 nm further shows equal absorbance of Az *trans* isomers across all polarization angles, signifying the random orientation of the Az in the

Table 1. Phase behavior and lattice parameters of the ODMS liquid crystals.[49]

	n	Phase behavior [°C] (Lattice parameters [nm])
LC-14Si	5	Col_{Rec} 109 (3.8, 7.4) Iso
LC-22Si	9	Col_{Rec} 49 (4.3, 8.5) Col_{Hex} 102 (4.5) Iso
LC-30Si	13	Col_{Hex} 95 (5.1) Iso

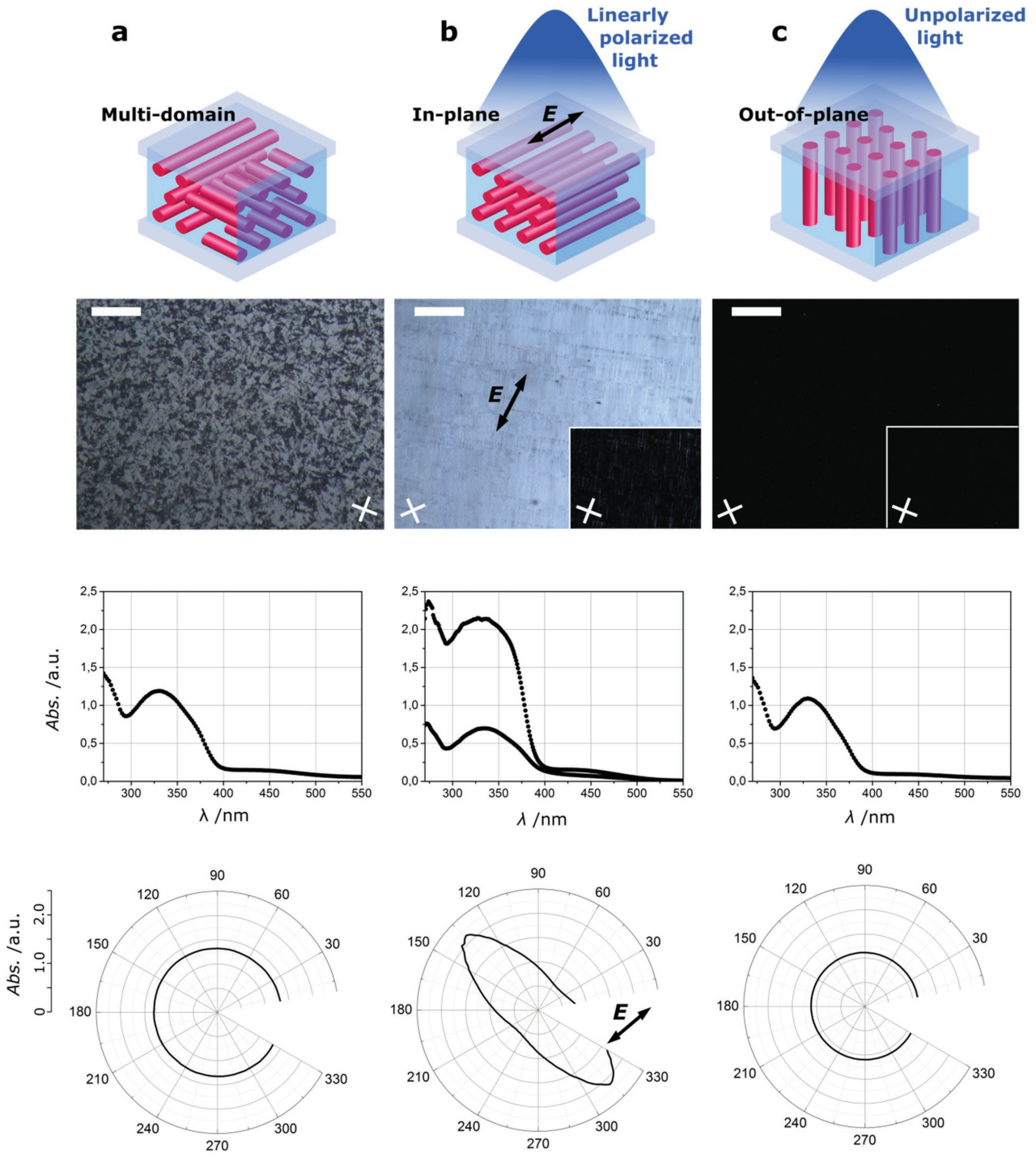

Figure 1. Schematic representations, room temperature POM images, room temperature polarized UV–vis absorption spectra, and corresponding polar plots, of LC-22Si contained in a quartz cell (≈1.5 µm) a) prior to photoalignment, b) after exposure to linearly polarized light, and c) after exposure to unpolarized light. The *E* direction is indicated by the arrow. The crosses represent the transmission axes of the crossed polarizers. All scale bars: 100 µm.

plane of the cell. Similar to the behavior in solution, exposure of the cell to unpolarized 365 nm UV light results in a decrease of the π–π^* transition absorption peak of the *trans* isomers at 330 nm, and an increase of the weaker n–π^* transition absorption peak of *cis* isomer at 439 nm (Figure S4, Supporting Information). Interestingly, the UV-exposed sample became an optically isotropic liquid, presumably due to a destabilization of the liquid crystal phase by bent-shaped *cis* isomers.[44,52–55] By exposure to 455 nm light or heat, the thermodynamically favored LC phase of the trans Az isomer was restored.

In order to verify if the cylindrical domains could be oriented through photoinduced *trans–cis–trans* isomerization cycles, the cell containing LC-22Si was subjected to 455 nm

LPL (Figure 1b), while cooling (0.1 °C min^{-1}) from the isotropic state to room temperature and then, in a subsequent experiment, to unpolarized 455 nm light (Figure 1c) under the same thermal cooling conditions. In the case of LPL, the POM texture after irradiation was highly anisotropic, extinguishing light when E was oriented at 0° and 90° relative to crossed polarizers. At 45° to the polarizers, the sample exhibited a bright state, indicative of the preferential orientation of the mesogens in a planar fashion. The corresponding polarized absorption measurements were used to calculate a dichroic ratio (DR) as $DR = (A_\perp - A_\parallel)/(A_\perp + A_\parallel)$, where $A_\perp$ and $A_\parallel$ represent the absorbance at the peak of the π–π^* transition band (330 nm), measured with polarized light perpendicular and parallel to E. For randomly oriented Azs, DR = 0, while for perfectly oriented Azs perpendicular to E, DR = 1. In this case, DR = 0.51, indicating that the Az moieties are on average oriented perpendicular to E,[51] though the moderate value suggests that there is disorder around the preferential orientation direction. However, X-ray diffraction (XRD) experiments (Figure S5, Supporting Information) reveal that the Az reorientation results in the alignment of the LC nanocylinders in a planar fashion (a = 4.5 nm) with the cylindrical axis parallel to E. Next, the out-of-plane alignment was investigated (Figure 1c) by irradiating with unpolarized 455 nm light. In this case, the POM texture no longer exhibited birefringence (optically isotropic), and no in-plane dichroism was induced (DR = 0). XRD experiments (Figure S5, Supporting Information) reveal a hexagonal symmetry in the scattering, originating from the vertical orientation of LC nanocylinders (a = 4.5 nm) in an essentially monodomain fashion. The out-of-plane cylinder orientation is characterized by a small decrease in the π–π^* transition absorption peak intensity when compared to the unaligned state and a large increase in absorption when the sample is tilted (Figure S6, Supporting Information), which suggest the Azs have partially turned parallel to the propagation direction of light in accordance to literature.[44,48,56] However, the significant remaining absorption intensity in the plane suggests that the effective photoinduced alignment of the azobenzene moieties perpendicular to the light polarization is compensated by a tendency of the Azs to align perpendicular to the axis of the cylinder. Interestingly, this suggests that only limited differences in the photoinduced Az orientation are responsible for the highly aligned LC mesophase morphologies in three dimensions, both in-plane (moderate DR) and out-of-plane (limited deviation from horizontal). Overall, these results show that light can be used to align the cylindrical mesophase morphology horizontally and vertically in a cell in a noncontact fashion. Furthermore, the photoinduced orientation, both at the chromophore and morphology levels, is stable at room temperature (RT) and may be erased and reoriented.

For most nanotechnology applications, the LC morphologies must be directed in sub-micrometer thin films. Therefore, LC thin films were prepared by spin-coating dilute solutions of liquid crystals in heptane onto quartz substrates modified with a poly(dimethylsiloxane) (PDMS) brush layer.[49,57] A 10 mg mL^{-1} solution of LC-22Si resulted in films of 40 nm thickness, as determined by ellipsometry. The film surface consists of multilayers of nanocylinders with a period of 4.3 nm (Figure S7, Supporting Information), corresponding to the room temperature Col_{Rec} phase (Table 1). Without an external driving force for alignment, the cylinders are planar oriented over arbitrary azimuthal angles in a multidomain fashion.[49] For the thin-film photoalignment experiments, the films were heated up close to the clearing temperature. **Figure 2**a–d shows 2D grazing-incidence X-ray diffraction (GIXRD) patterns of the LC-22Si thin film at 85 °C (Col_{Hex} phase, Table 1), before and after exposure to unpolarized light and LPL of 455 nm (1 h, 0.6 J cm^{-2} min^{-1}). In each case, the broad reflections at 7 $nm^{-1} < q < 14$ nm^{-1} signify that the liquid-like nature of the respective intermolecular interactions (siloxane–siloxane and organic–organic) is maintained. Before photoalignment (Figure 2a), periodic (q, $\sqrt{3}q$, $2q$) scattering peaks were observed at q = 1.68, 2.90, and 3.36 nm^{-1}, corresponding to the Col_{Hex} phase (a = 4.5 nm). The primary scattering peaks corresponding to the {1 0} planes were observed at azimuthal angles $\varphi \approx 30°$, $\varphi \approx 90°$, and $\varphi \approx 150°$, confirming that the self-assembly is exclusively in-plane. After exposure to unpolarized light (Figure 2b), the periodicity remained at 4.5 nm, while the primary scattering peak appeared at azimuthal angles $\varphi \approx 0°$, $\varphi \approx 180°$ and the in-plane scattering greatly diminished. These data suggest that the effect of unpolarized light is the re-orientation from in-plane cylinders to predominantly out-of-plane cylinders. However, it should be noted that the out-of-plane morphology could not be retained in thin films upon cooling to room temperature (vide infra). In contrast, Figure 2c,d depicts GIXRD measurements recorded parallel (Figure 2c) and perpendicular (Figure 2d) to the E direction of LPL. Parallel to E, the diffraction pattern exhibits many higher order reflections corresponding to a hexagonal columnar lattice with high positional order. The periodicity remained at 4.5 nm. Perpendicular to E, the diffraction exhibits the total absence of reflections at $\varphi \approx 30°$ and $\varphi \approx 150°$. Scattering intensity is preserved only at the azimuthal angle of $\varphi \approx 90°$. Together, this is consistent with the presence of vertically stacked layers of nanocylinders in which the cylinder axes are exclusively parallel to the E. The aligned sample was subsequently cooled to room temperature (Col_{Rec} phase). Polarized UV–vis measurements (Figure S8, Supporting Information) confirm that the corresponding alignment of Az moieties is perpendicular to the E direction (DR = 0.71), consistent with the results found in bulk (Figure 1b). These findings suggest that the Az moieties are, on average, perpendicular to the columnar axis, and the effect of LPL is the net orientation of LC cylinders parallel to E. In order to confirm these findings, high-resolution atomic force microscopy (AFM) was performed in tapping mode. Figure 2e shows an AFM phase image, which exhibits a monoaxial array of periodic line structures with a periodicity of 4.3 nm. The LC cylinders are oriented parallel to the E direction, in accordance with the GIXRD data at 85 °C, indicating that the aligned planar morphology can be retained upon cooling to room temperature. Remarkably, there are no observable nonequilibrium defects that are usually found in photoaligned glassy BCP systems,[36,38,58] despite the value of DR to achieve this (DR = 0.71) differs from that of a perfectly ordered Az system (DR = 1).[40] Furthermore, optical microscopy (Figure S9, Supporting Information)

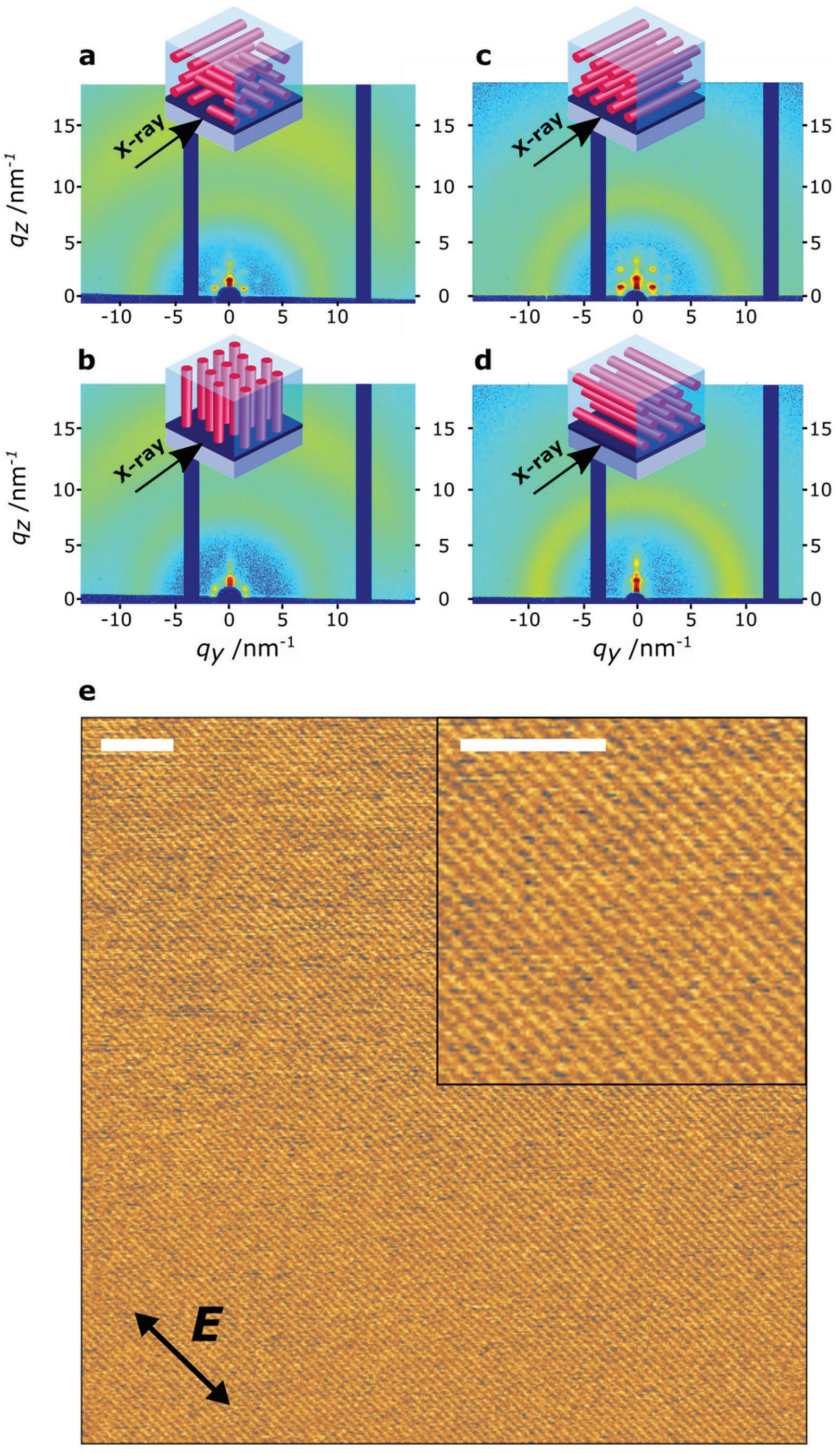

Figure 2. Thin-film photoalignment of AzoLC-22Si: 2D GIWAXS profiles a) before photoalignment, b) after photoalignment with unpolarized light, and after photoalignment with LPL measured c) parallel and d) perpendicular to *E*. e) High-resolution phase-mode AFM image of a planar aligned sample. The polarization direction of the LPL is indicated by the arrow. The inset corresponds to a 2× magnification. Scale bars: 50 nm.

reveals that the photoaligned thin films consist of large anisotropic domains which extend hundreds of micrometers in the direction parallel to *E*. Together, these results show that the alignment of LC cylinders can be achieved across large areas in sub-5 nm patterned thin films, and their 3D orientation can be controlled. However, in contrast to the behavior in a cell (Figure 1c), the out-of-plane morphology could not be retained in thin films, indicating the prominence of surface energy contributions to the free energy.[58]

In order to gain insight into the 3D photoalignment process, thicker films were prepared (≈150 nm), allowing combined time-resolved polarized UV–vis absorption spectroscopy and GIXRD measurements to correlate the orientation of photoresponsive azobenzene moieties with the alignment of the cylinders in time. First, the in-plane orientation at regular intervals (1 min, 0.6 J cm^{-2} min^{-1}), during an initial alignment (5 min) and a subsequent orthogonal realignment process (10 min) was studied. In each case, the photoalignment was performed at 85 °C. For UV–vis absorption spectroscopy, the samples were quickly cooled to room temperature and at each interval, DR was calculated. In this case, the direction of *E* in the second exposure was chosen as the reference direction.[38] For randomly oriented Azs, DR = 0, while for perfectly oriented Azs along the first and second alignment directions, DR becomes –1 and +1, respectively. **Figure 3** shows the angular dependence of azobenzene absorbance at selected times during the alignment procedure. No optical anisotropy was observed prior to exposure to LPL (Figure 3a, DR = 0). After a 5 min LPL exposure (3.0 J cm^{-2}), the azobenzene absorbance became highly anisotropic; with increased absorbance perpendicular to *E* and decreased absorbance in the parallel direction (Figure 3b, DR = –0.56). The sample was subsequently subjected to a second LPL irradiation in the orthogonal direction. After a 1 min LPL exposure (0.6 J cm^{-2}), the polar plot regained its circular shape representing the almost complete loss of optical anisotropy (Figure 3c) (DR = –0.12). After a 5 min LPL exposure (3.0 J cm^{-2}), the optical anisotropy was almost completely regained in the direction orthogonal to the initial direction (Figure 3d, DR = 0.53). The change in sign is representative for the change in orientation of the Az mesogens upon exposure in the orthogonal direction, and demonstrates the feasibility of the alignment process in arbitrary directions.

GIXRD was used to examine the time-course evolution of the orientation of LC cylinders during the alignment and the subsequent re-alignment process. Similar to the UV–vis experiments (Figure 3), the sample was irradiated at 85 °C, and data were collected over 1 min intervals (0.6 J min^{-1} cm^{-2}).

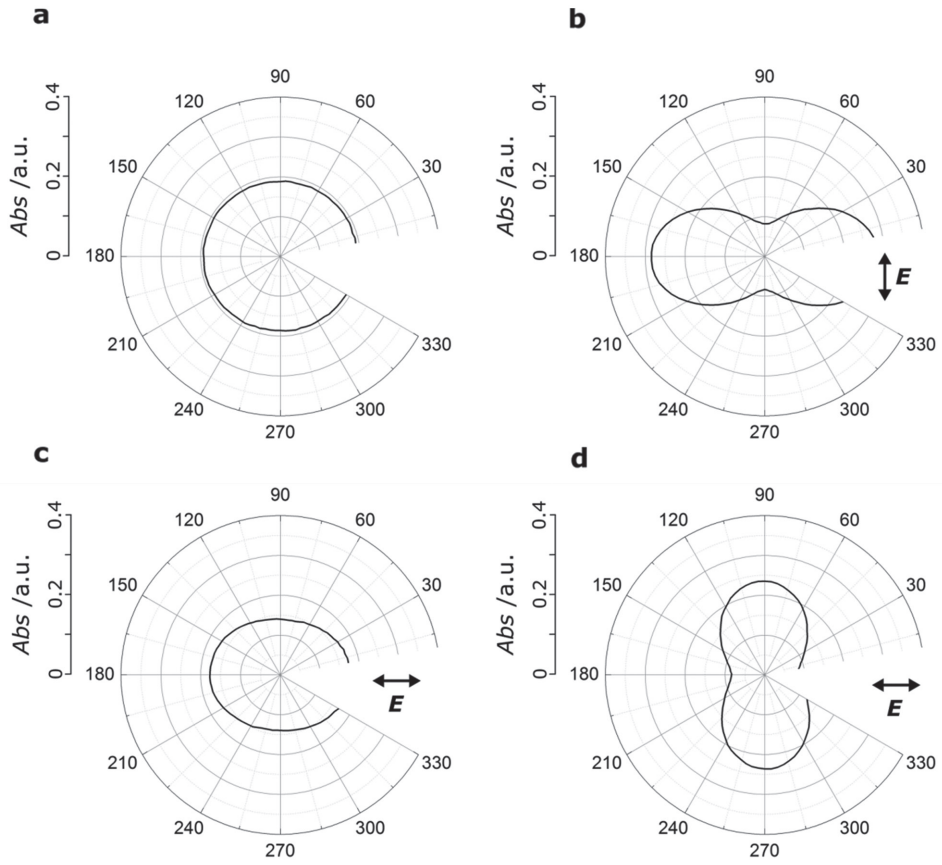

Figure 3. Room-temperature polarized UV–vis spectroscopic data for an LC-22Si thin film aligned using linearly polarized light at 85 °C (0.6 J cm^{-2} min^{-1}). Polar plots are shown for the film a) before irradiation, b) after the first 5 min LPL irradiation, c) after a short 1 min perpendicular LPL irradiation, and d) after a 5 min perpendicular LPL irradiation. The electric field vector of the LPL is indicated by the arrow.

The measurements were performed using two orthogonal X-ray incident directions (beam 1, beam 2), which were parallel to the *E* of the LPL in the first and the second exposure, respectively. **Figure 4** presents representative snapshots of the 2D scattering images collected before irradiation (a), after the first 5 min LPL irradiation (3.0 J cm^{-2}) (b), and after a second 5 min perpendicular LPL irradiation (3.0 J cm^{-2}) (c). Before irradiation, the scattering intensity was independent of the incident direction of the X-rays, signifying the initial multidomain state of the film (Figure 4a). During the course of the first LPL irradiation, beam 1 resulted in increased scattering at azimuthal angle $\varphi \approx 30°$ and $\varphi \approx 150°$, while beam 2 resulted in a fast loss of scattering (Figure 4b). These features are indicative of the photoinduced monoaxial alignment of hexagonally well-packed LC cylinders parallel to *E*. Subsequent irradiation in the orthogonal direction resulted in the inverse situation (Figure 4c). Scattering at azimuthal angle $\varphi \approx 90°$ is maintained in all cases, consistent with the preservation layers of nanocylinders stacked in the plane.

To further examine the correlation between the polarized UV–vis spectroscopic data related to the azobenzene orientation (Figure 3) and the GIXRD measurements related to the LC nanocylinder orientation (Figure 4), over the course of the initial alignment (5 min) and subsequent orthogonal realignment (20 min) process, the data are plotted together in **Figure 5**. For simplicity we now refer to the second realignment process (beyond the dotted line in Figure 5). The DR, shown in Figure 5a, climbs exponentially from a negative to a positive value. The signal is almost saturated after 5 min. No lag period was resolved, indicating that the photostationary state is reached rapidly under these conditions (455 nm irradiation, 0.6 J min^{-1} cm^{-2}). The photostationary state is also accompanied by a decrease in GIXRD scattering intensity at azimuthal angle $\varphi \approx 90°$ (Figure S10, Supporting Information), signifying a reduction in local LC order due to the ongoing photoisomerization. The average GIXRD scattering intensities at azimuthal angle $\varphi \approx 30°$ and $\varphi \approx 150°$, which were obtained perpendicular (closed circles) (beam 1) and parallel (open circles) (beam 2) to the incidence of the LPL in the second alignment step, are plotted in Figure 5b. In the perpendicular direction (beam 1), the signal decays immediately after irradiation, and is lost rapidly (≈5 min). The loss in scattering intensity rapidly follows the change in DR. In the parallel direction (beam 2), a short lag period is observed, and the signal continues to increase over a longer period (≈20 min). This observation is different from previously reported observations for BCPs,[38] in which the GIXRD intensity rises only after the DR has saturated. This finding suggests that the LCs are mostly re-oriented within the first few minutes (≈5 min), and that the subsequent rise in GIXRD intensity likely corresponds to the fusion of separate re-oriented subdomains to form a monodomain. The faster

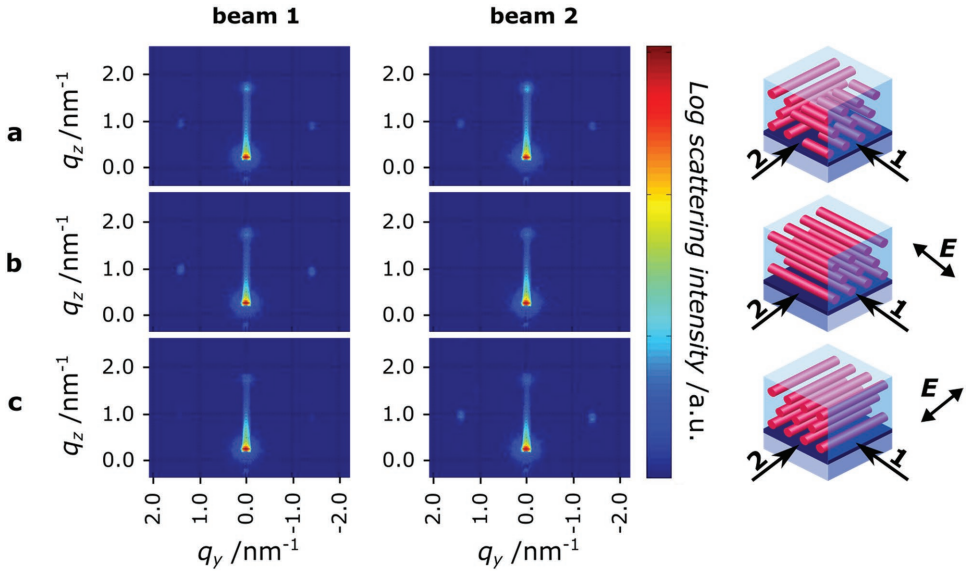

Figure 4. Snapshots of the 2D GIXRD profiles for the LC-22Si thin film aligned using LPL at 0.6 J min^{-1} cm^{-2}, collected a) before irradiation, b) after the first 5 min LPL irradiation (3.0 J cm^{-2}), and c) after a second 5 min perpendicular LPL irradiation (3.0 J cm^{-2}), obtained using two orthogonal X-ray incident directions (beam 1, beam 2). The *E* is indicated by the arrow.

dynamics in our system may be the result of the high mobility and low viscosity of the low-molecular-weight liquid crystalline phase.

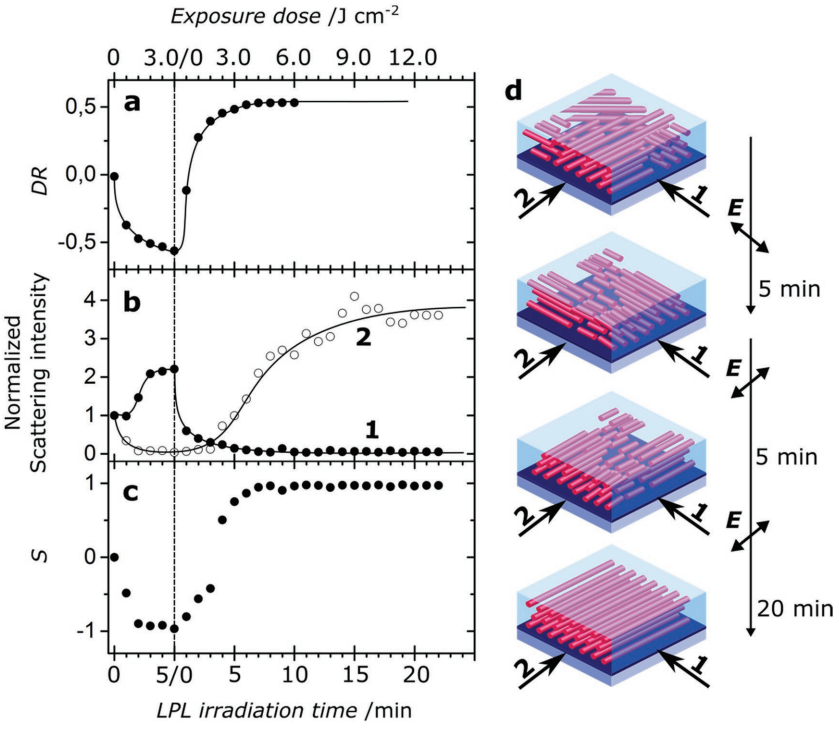

Figure 5. Time-course profiles of the a) dichroic ratio DR, b) average GIXRD scattering intensities at azimuthal angles $\varphi \approx 30°$ and $\varphi \approx 150°$ measured perpendicular (closed circles) (beam 1) and parallel (open circles) (beam 2) to the incidence of the LPL in the second exposure, c) order parameter *S* of the cylinders, and d) schematic representations of the nanocylinder orientation at various times in the alignment procedure as a function of the irradiation time and exposure dose, for the LC-22Si thin film aligned using LPL at 0.6 J min^{-1} cm^{-2}. The *E* and beam directions are indicated by the arrows.

In order to more directly compare DR with the GIXRD intensities, an order parameter of the cylinders was calculated as $S = (I_1 - I_2)/(I_1 + I_2)$, with I_1 and I_2 being the average of the scattering intensities at azimuthal angles $\varphi \approx 30°$ and $\varphi \approx 150°$, recorded with beam 1 and beam 2, respectively. Similar to DR, for randomly aligned cylinders $S = 0$, while for perfectly aligned cylinders along directions 1 and 2, the order parameter becomes –1 and +1, respectively. Figure 5c shows that the trend of *S* is closely coupled to that of the DR. Hence, the change in order of the cylinders is coupled to the change in Az orientation. It is indeed expected that the nanocylinder order is more closely linked to the Az order (DR) than in the previously studied BCP system for this purpose,[38] since the Azs are directly contained within the cylinder nanostructures, as opposed to the forming part of the surrounding matrix material.[36–42] In contrast to the DR, *S* reaches the theoretical minimum (–1) and maximum (1) values, representative for a perfectly ordered system. In other words, despite the fact that the Az moieties show a local disorder around the preferential orientation direction (moderate DR), the degree of alignment of the self-assembled cylinders is very high (maximum *S*).

It is expected that the temperature has a significant effect on the self-assembly processes during the photoalignment procedure. In order to further elucidate this, the effects of temperature and the clearing temperature were investigated.

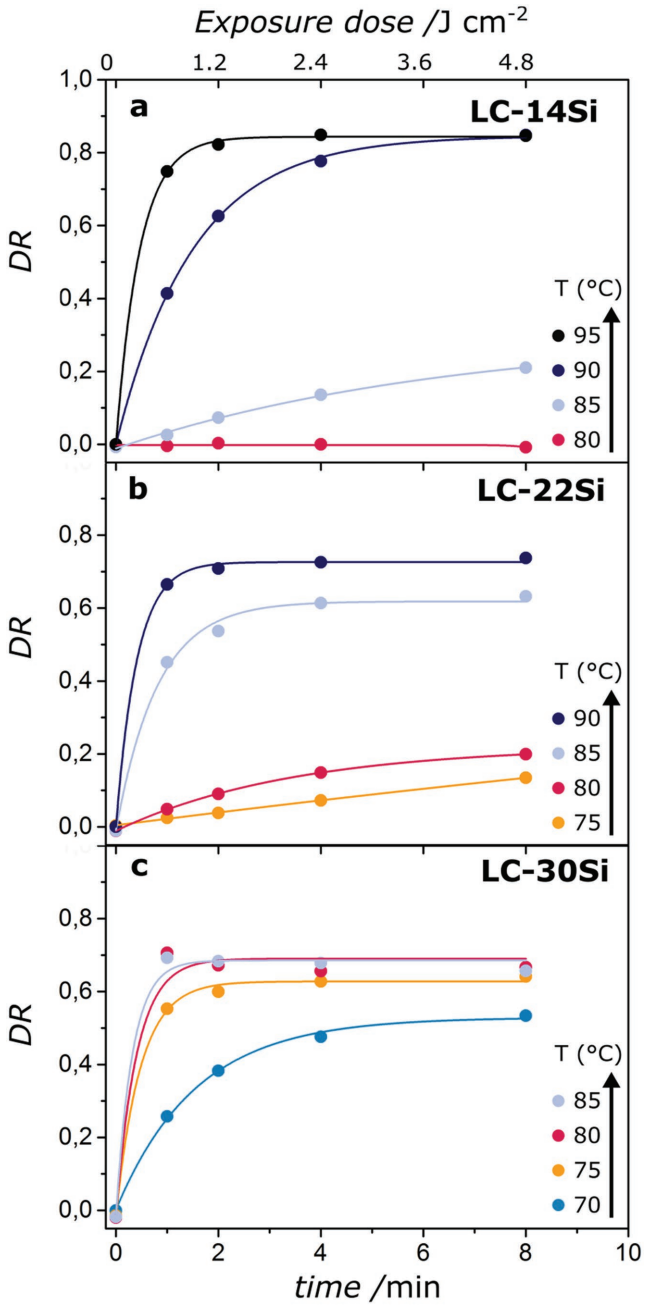

Figure 6. Polarized UV–vis spectroscopic data for a) LC-14Si, b) LC-22Si, and c) LC-30Si thin films aligned at various temperatures using linearly polarized light at 0.6 J min^{-1} cm^{-2}. The irradiation time and the corresponding dose are indicated in the graphs. The lines correspond to exponential saturation fits.

Figure 6 shows the time evolution of DR for LC-14Si, LC-22Si, and LC-30Si, exposed to LPL at 0.6 J cm^{-2} min^{-1}, at temperatures between 70 and 95 °C. In order to describe the phenomena and allow comparison of the different experiments and materials, the DR evolution was fitted to a single exponential saturation function $DR = DR_{max}(1 - e^{-t/\tau})$, in which DR_{max} is the calculated dichroic ratio after infinite exposure, t is the exposure time (min), and τ is the characteristic time to reach saturation (min). In order to more accurately compare the different LCs, the fitted alignment parameters were plotted as a function of the reduced temperature $T_R = T/T_C$, with T_C being the clearing temperature of the (all *trans*) liquid crystal (Figure S11, Supporting Information).

For LC-14Si, no order is photoinduced for temperatures below 80 °C ($DR_{max} = 0$). At 85 °C, there is a limited induction of order (= 0.31), and at 90 and 95 °C a high degree of Az order is achieved around the preferential alignment direction ($DR_{max} = 0.84$). In contrast, LC-30Si reaches saturation DR values, which are not so dependent on temperature, at the whole explored temperature range from 70 °C ($DR_{max} = 0.52$) to 85 °C ($DR_{max} = 0.70$). LC-22Si represents the intermediate case. The characteristic times (Figure S11b, Supporting Information) are also a function of temperature, with very fast alignment just under T_C ($T_R > 0.85$), and slower molecular order buildup at lower temperatures. Also in this case, the dependence is less marked in the large ODMS chain material LC-30Si. For each of the LCs, dewetting of the film occurred close to the clearing point ($T_R > 0.9$), which was observed by a decreased overall UV–vis absorbance. Likely, the point of dewetting coincides with the effective clearing temperature under irradiation, which is reduced by the presence of *cis* isomers in the photostationary state (Figure S4, Supporting Information) and concurrent photofluidization by irradiation (Figure S10, Supporting Information) to result in a more mobile isotropic phase.

Together, it is observed that the highest degree of order (high DR_{max}) can be achieved fast (low τ) just below the dewetting conditions (Figure S11, Supporting Information), where the system has the highest mobility, which suggests that the dominant energetic barrier in the alignment process is the destabilization of the LC domains.[38,59] Moreover, the processing window for an optimal alignment is broadened by increased ODMS fractions (LC-14Si < LC-22Si < LC-30Si), which is in agreement with the observation that higher ordered phases are more able to resist photoinduced perturbation.[42] Combined with the observations of a lower T_C and a lower DR_{max} (at the optimum T conditions, just below the dewetting conditions) for increased ODMS fractions, this suggests that the ODMS lowers the packing ability of Az moieties within each cylinder, and hence, lowers the energetic barrier to domain destabilization required for alignment. Perhaps counterintuitively, this means that the lower order of Az moieties within the cylinders could be beneficial toward achieving a more effective alignment of nanostructures on a larger length scale.

Finally, the out-of-plane alignment process was investigated by GIXRD for a thin film (≈150 nm) of LC-30Si (**Figure 7**), which was selected for its comparatively larger processing window (Figure S11, Supporting Information). Prior to irradiation and at room temperature, azimuthal integration around the primary reflection (1.45 nm^{-1} < q < 1.55 nm^{-1}) (Figure 7a) results in a strong signal at $\varphi = 30°$, stemming from the in-plane oriented LC cylinders. The LC film was subsequently exposed to unpolarized light (455 nm, 0.6 J min^{-1} cm^{-2}) at various temperatures and for extended periods (60 min) to ensure that equilibrium was reached. At 75 °C, the reflections are broadened (Figure 7b), suggesting that the in-plane domains are perturbed and

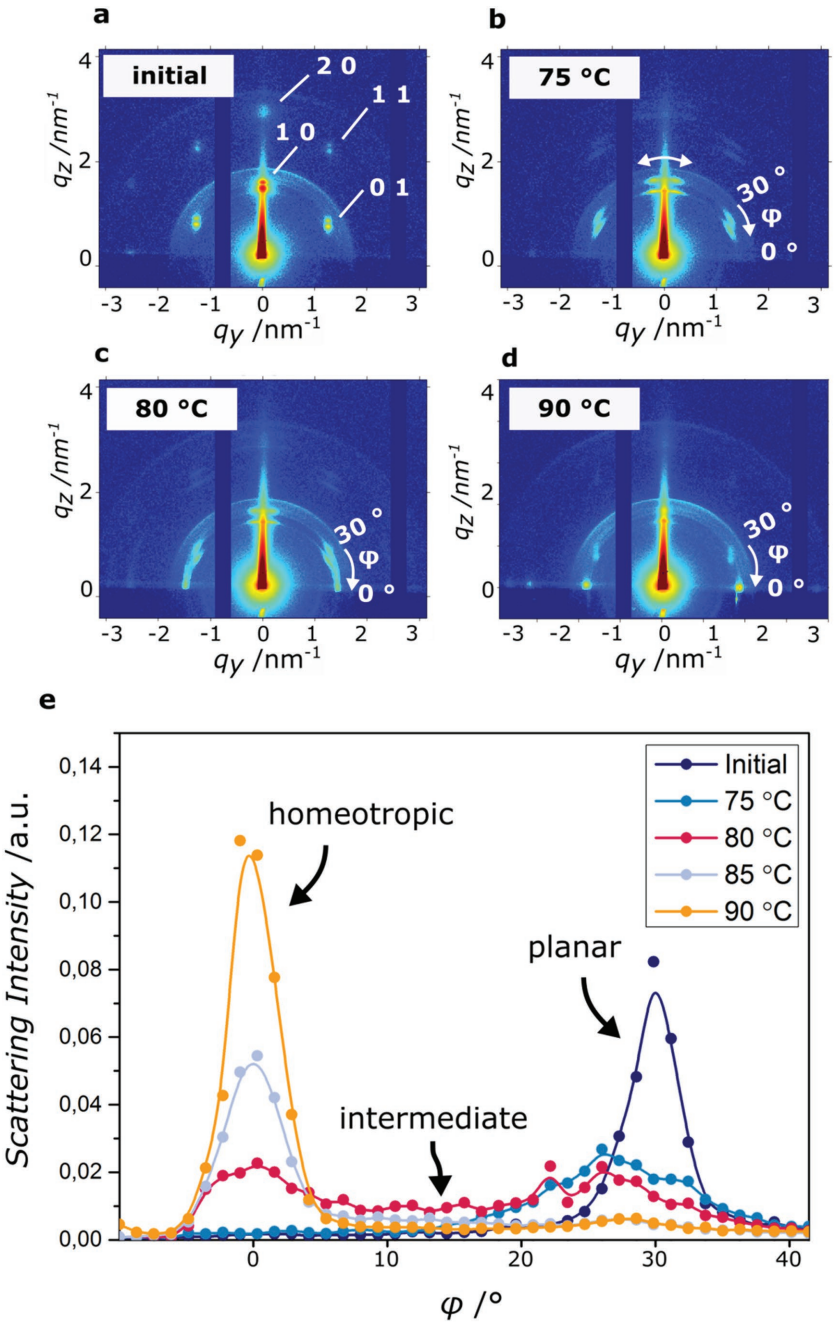

Figure 7. Out-of-plane alignment with unpolarized light: 2D GIXRD profiles of an LC-30Si thin film in a) the initial state at 25 °C and b–d) after photoalignment with unpolarized light at various temperatures. e) Azimuthal integration over the primary (1 0) reflection.

their orientation is less well defined. This effect is further highlighted by the greatly diminished diffraction intensity of the first order (1 0) (q = 1.51 nm^{-1}) and second order (2 0) (q = 2.96 nm^{-1}) reflections perpendicular to the substrate (q_y = 0) (Figure S12, Supporting Information). At 80 °C, this effect becomes more pronounced, and additional reflections appear at $\varphi = 0°$ (Figure 7e), where $q_z = 0$ (Figure S12, Supporting Information). The reflections are situated at q = 1.51 nm^{-1}, q = 2.54 nm^{-1}, and q = 2.93 nm^{-1}, which are indexed as the (0 1), (1 1), and (0 2) reflections, respectively, indicating unequivocally the presence of out-of-plane orientated LC cylinder domains.[33,60] These domains are present alongside in-plane oriented domains (Figure 7e), and hence this state is intermediate. At higher temperatures, the fraction of out-of-plane domains is increased. At 90 °C, the intensity corresponding to the in-plane oriented domains is significantly diminished, indicating that the domains are almost exclusively out-of-plane (Figure 7d). At 95 °C, a drop in scattering intensity from all reflections was observed, likely due to the dewetting of the film (data not shown). Similar to the in-plane alignment, the optimal temperature for out-of-plane photoalignment is just under T_C. However, when compared to the in-plane alignment of LC cylinders, it is clear that the processing window for obtaining out-of-plane oriented LC cylinders is much more narrow. Finally, after halting the irradiation and cooling down to room temperature, the out-of-plane alignment returned to an in-plane alignment (Figure S13, Supporting Information), an interface effect which has been observed in previous studies.[60,61] These findings suggest a strong competition between the photoinduced out-of-plane orientation and the thermodynamically stable in-plane orientation. It shows that obtaining the out-of-plane orientation of cylinders is challenging due to the intrinsic surface energy mismatch between the mesogenic core and ODMS coils.[49,62]

3. Conclusion

In conclusion, highly ordered sub-5 nm nanocylinder arrays were obtained over large areas by the photoalignment of Az-containing liquid crystals. By using linearly polarized light, in-plane oriented nanocylinders were obtained in thin films. The in-plane photoalignment was shown to proceed by a mechanism in which the nanocylinders are rapidly oriented, followed by fusion and growth of the re-oriented domains into a monodomain. When performed just under the clearing temperature of the LC phase, the photoalignment was demonstrated to proceed most efficiently, reaching completion within minutes. Since the Azs are contained directly in the cylinder nanostructures, the dichroism and nanocylinder order follow the same trend and appear closely linked. However, due to local disorder on the Az length scale, only a moderate dichroism is required to achieve high order on the length scale of the nanostructures. Interestingly, while the local Az order decreases with increasing ODMS content in the LC series, this broadens the temperature processing window with which aligned nanostructures

can be achieved. Additionally, the LC nanocylinders could be oriented out-of-plane by exposure to unpolarized light, which is a promising alternative to solvent annealing[63] or surface layers.[64,65] However, while stable out-of-plane nanostructures were obtained in a cell, the morphology was not retained in thin films. Obtaining stable out-of-plane orientations remains challenging,[66] particularly for high-etch contrast small molecules such as this. Chemical crosslinking[35] or cooling through a glass transition[36] is a possible solution. Overall, our results pave the way for generating defect-free sub-5 nm patterned thin films with 3D orientational control by light. For integrated circuit production, in particular, the LC mobility could be key to achieving both the low defect tolerance[4] and fast alignment for high wafer throughput.[18] Moreover, the planar photoalignment could be extended to the micro-patterning of distinct domain orientations or be applied in combination with other alignment methods to achieve the stringent lithography specifications required at future technology nodes.[67,68]

4. Experimental Section

Materials: The synthesis and characterization of the oligo(dimethylsiloxane) liquid crystals can be found in a previous report.[49]

Thin-Film Preparation: A hydroxy-terminated PDMS homopolymer from Polymer Source with molecular weight 5 kg mol^{-1} was applied onto quartz substrates from a 1–2 wt% solution in heptane, baked at 150 °C for at least 24 h, and rinsed with heptane. The liquid crystals were subsequently spin-coated from 10 or 30 g L^{-1} solution in heptane (3000 rpm, 45 s), resulting in film thicknesses of ≈40 and 150 nm, as determined by ellipsometry.

Photoalignment of LCs: Linearly polarized light was obtained from a 455 nm light-emitting diode (LED) (Thorlabs) equipped with a dichroic polarizing sheet (Polarizer Sheet XP44—Linear Polarizer; ITOS GmbH, Mainz, Germany). The light intensity was 10.0 mW cm^{-2}. For bulk photoalignment, the samples were heated to the isotropic phase and then slowly cooled (0.1 °C min^{-1}) under irradiation. In thin films, the photoalignment was performed below the LC clearing temperature to avoid dewetting. Unless otherwise indicated, the thin-film photoalignment was performed at 85 °C.

X-Ray Scattering: X-ray scattering measurements were performed on a Ganesha lab instrument equipped with a GeniX-Cu ultralow divergence source producing X-ray photons with a wavelength of 1.54 Å and a flux of 1×10^8 ph s^{-1}. Scattering patterns were collected using a Pilatus 300 K silicon pixel detector. The beam center and the q range were calibrated using the diffraction peaks of silver behenate. Bulk XRD was performed on samples sealed in a 1 mm glass capillary. GIXRD was performed at the critical angle (≈0.16°). This resulted in shadow peaks at higher q due to reflection + diffraction events just above the critical angle. The sample-to-detector distance was 91 mm for wide-angle measurements and 441 mm for medium-angle measurements. For the experiment using orthogonal beams, the results of two experiments performed under identical photoalignment conditions but at a 90° angle with respect to each other were combined. Time-resolved measurements were the average of 60 s of exposure.

AFM Measurements: The AFM data were recorded in ambient conditions using a Dimension ICON atomic force microscope (Bruker Nano Inc., Santa Barbara, CA) fitted with an NCHV silicon probe (Bruker, spring constant 42 N m^{-1}, and a resonance frequency of 320 kHz).

Supporting Information

Supporting Information is available from the Wiley Online Library or from the author.

Acknowledgements

The authors would like to thank S. Wuister, C. van Lare, and T. Druzhinina from ASML for general support and the provision of quartz wafers, B. de Waal for ODMS synthesis, and B. Meijer and D. Broer for discussions. This research was supported by the Dutch Technology Foundation STW, which is part of the Netherlands Organisation for Scientific Research (NWO), and which is partly funded by the Ministry of Economic Affairs. C.S.-S. thanks the Spanish MINECO projects MAT2011-27978-C02-02, SAF2014-54763-C2-2-R, Gobierno de Aragón, and FEDER (EU). P.L. is a Senior Research Associate from FRS-FNRS (Belgium). The X-ray diffractometer was financed by The Netherlands Organisation for Scientific Research (NWO).

Conflict of Interest

The authors declare no conflict of interest.

[1] C. M. Bates, M. J. Maher, D. W. Janes, C. J. Ellison, C. G. Willson, *Macromolecules* **2014**, *47*, 2.
[2] A. Nunns, J. Gwyther, I. Manners, *Polymer* **2013**, *54*, 1269.
[3] S.-J. Jeong, J. Y. Kim, B. H. Kim, H.-S. Moon, S. O. Kim, *Mater. Today* **2013**, *16*, 468.
[4] J. Bang, U. Jeong, D. Y. Ryu, T. P. Russell, C. J. Hawker, *Adv. Mater.* **2009**, *21*, 4769.
[5] S.-M. Yang, S. G. Jang, D.-G. Choi, S. Kim, H. K. Yu, *Small* **2006**, *2*, 458.
[6] X. Yu, K. Yue, I. F. Hsieh, Y. Li, X. H. Dong, C. Liu, Y. Xin, H. F. Wang, A. C. Shi, G. R. Newkome, R. M. Ho, E. Q. Chen, W. B. Zhang, S. Z. Cheng, *Proc. Natl. Acad. Sci. USA* **2013**, *110*, 10078.
[7] Y. H. Kim, D. K. Yoon, H.-T. Jung, *J. Mater. Chem.* **2009**, *19*, 9091.
[8] C. Tschierske, *J. Mater. Chem.* **2001**, *11*, 2647.
[9] C. Tschierske, *Angew. Chem. Int. Ed.* **2013**, *52*, 8828.
[10] J. V. Barth, G. Costantini, K. Kern, *Nature* **2005**, *437*, 671.
[11] G. M. Whitesides, B. Grzybowski, *Science* **2002**, *295*, 2418.
[12] C. L. Gonzalez, C. W. M. Bastiaansen, J. Lub, J. Loos, K. Lu, H. J. Wondergem, D. J. Broer, *Adv. Mater.* **2008**, *20*, 1246.
[13] M. Zhou, T. J. Kidd, R. D. Noble, D. L. Gin, *Adv. Mater.* **2005**, *17*, 1850.
[14] X. D. Feng, M. E. Tousley, M. G. Cowan, B. R. Wiesenauer, S. Nejati, Y. Choo, R. D. Noble, M. Elimelech, D. L. Gin, C. O. Osuji, *ACS Nano* **2014**, *8*, 11977.
[15] B. R. Kaafarani, *Chem. Mater.* **2011**, *23*, 378.

[16] R. Ruiz, H. M. Kang, F. A. Detcheverry, E. Dobisz, D. S. Kercher, T. R. Albrecht, J. J. de Pablo, P. F. Nealey, *Science* **2008**, *321*, 936.
[17] T. Thurn-Albrecht, J. Schotter, C. A. Kastle, N. Emley, T. Shibauchi, L. Krusin-Elbaum, K. Guarini, C. T. Black, M. T. Tuominen, T. P. Russell, *Science* **2000**, *290*, 2126.
[18] S. Park, D. H. Lee, J. Xu, B. Kim, S. W. Hong, U. Jeong, T. Xu, T. P. Russell, *Science* **2009**, *323*, 1030.
[19] C. Sinturel, F. S. Bates, M. A. Hillmyer, *ACS Macro Lett.* **2015**, *4*, 1044.
[20] C. M. Bates, F. S. Bates, *Macromolecules* **2017**, *50*, 3.
[21] H. Siebert, I. Quijada-Garrido, J. Vermant, L. Noirez, W. R. Burghardt, C. Schmidt, *Macromol. Chem. Phys.* **2007**, *208*, 2161.
[22] R. H. Zha, B. F. de Waal, M. Lutz, A. J. Teunissen, E. W. Meijer, *J. Am. Chem. Soc.* **2016**, *138*, 5693.
[23] J. C. Wittmann, P. Smith, *Nature* **1991**, *352*, 414.
[24] M. Hara, S. Nagano, T. Seki, *J. Am. Chem. Soc.* **2010**, *132*, 13654.
[25] H. K. Bisoyi, Q. Li, *Chem. Rev.* **2016**, *116*, 15089.
[26] K. Ichimura, *Chem. Rev.* **2000**, *100*, 1847.
[27] T. Seki, *J. Mater. Chem. C* **2016**, *4*, 7895.
[28] Y. Zakrevskyy, J. Stumpe, C. F. J. Faul, *Adv. Mater.* **2006**, *18*, 2133.
[29] S. Pan, M. Ni, B. Mu, Q. Li, X.-Y. Hu, C. Lin, D. Chen, L. Wang, *Adv. Funct. Mater.* **2015**, *25*, 3571.
[30] H. Monobe, K. Awazu, Y. Shimizu, *Adv. Mater.* **2006**, *18*, 607.
[31] O. Yaroshchuk, Y. Reznikov, *J. Mater. Chem.* **2011**, *22*, 286.
[32] D. K. Yoon, S. R. Lee, Y. H. Kim, S.-M. Choi, H.-T. Jung, *Adv. Mater.* **2006**, *18*, 509.
[33] K. Kwon, J. M. Ok, Y. H. Kim, J.-S. Kim, W.-B. Jung, S.-Y. Cho, H.-T. Jung, *Nano Lett.* **2015**, *15*, 7552.
[34] J. Cattle, P. Bao, J. P. Bramble, R. J. Bushby, S. D. Evans, J. E. Lydon, D. J. Tate, *Adv. Funct. Mater.* **2013**, *23*, 5997.
[35] X. Feng, S. Nejati, M. G. Cowan, M. E. Tousley, B. R. Wiesenauer, R. D. Noble, M. Elimelech, D. L. Gin, C. O. Osuji, *ACS Nano* **2016**, *10*, 150.
[36] Y. Morikawa, T. Kondo, S. Nagano, T. Seki, *Chem. Mater.* **2007**, *19*, 1540.
[37] K. Fukuhara, Y. Fujii, Y. Nagashima, M. Hara, S. Nagano, T. Seki, *Angew. Chem. Int. Ed.* **2013**, *52*, 5988.
[38] M. Sano, S. Nakamura, M. Hara, S. Nagano, Y. Shinohara, Y. Amemiya, T. Seki, *Macromolecules* **2014**, *47*, 7178.
[39] T. Seki, *Polym. J.* **2014**, *46*, 751.
[40] H. F. Yu, T. Iyoda, T. Ikeda, *J. Am. Chem. Soc.* **2006**, *128*, 11010.
[41] T. Seki, *Macromol. Rapid Commun.* **2014**, *35*, 271.
[42] M. Sano, M. Hara, S. Nagano, Y. Shinohara, Y. Amemiya, T. Seki, *Macromolecules* **2015**, *48*, 2217.
[43] K. M. Lee, T. J. White, *Macromolecules* **2012**, *45*, 7163.
[44] T. Ikeda, *J. Mater. Chem.* **2003**, *13*, 2037.
[45] H. Yu, *J. Mater. Chem. C* **2014**, *2*, 3047.
[46] S. Nagano, *Chem. Rec.* **2016**, *16*, 378.
[47] S. Nagano, Y. Koizuka, T. Murase, M. Sano, Y. Shinohara, Y. Amemiya, T. Seki, *Angew. Chem. Int. Ed.* **2012**, *51*, 5884.
[48] K. Ichimura, S. Morino, H. Akiyama, *Appl. Phys. Lett.* **1998**, *73*, 921.
[49] K. Nickmans, J. N. Murphy, B. de Waal, P. Leclère, J. Doise, R. Gronheid, D. J. Broer, A. P. H. J. Schenning, *Adv. Mater.* **2016**, *28*, 10068.
[50] K. Gao, H.-H. Cheng, A. K. Bhowmik, P. J. Bos, *Opt. Express* **2015**, *23*, 26086.
[51] A. Natansohn, P. Rochon, *Chem. Rev.* **2002**, *102*, 4139.
[52] J. Garcia-Amoros, A. Szymczyk, D. Velasco, *Phys. Chem. Chem. Phys.* **2009**, *11*, 4244.
[53] S. Xie, A. Natansohn, P. Rochon, *Chem. Mater.* **1993**, *5*, 403.
[54] C. Sanchez, R. Alcala, S. Hvilsted, P. S. Ramanujam, *J. Appl. Phys.* **2003**, *93*, 4454.
[55] T. Ikeda, S. Horiuchi, D. B. Karanjit, S. Kurihara, S. Tazuke, *Macromolecules* **1990**, *23*, 36.
[56] N. Kawatsuki, H. Takatsuka, T. Yamamoto, *Jpn. J. Appl. Phys.* **2000**, *39*, L230.
[57] Y. S. Jung, C. A. Ross, *Nano Lett.* **2007**, *7*, 2046.
[58] Y. Morikawa, S. Nagano, K. Watanabe, K. Kamata, T. Iyoda, T. Seki, *Adv. Mater.* **2006**, *18*, 883.
[59] A. V. Bogdanov, A. K. Vorobiev, *J. Phys. Chem. B* **2013**, *117*, 13936.
[60] E. Pouzet, V. D. Cupere, C. Heintz, J. W. Andreasen, D. W. Breiby, M. M. Nielsen, P. Viville, R. Lazzaroni, G. Gbabode, Y. H. Geerts, *J. Phys. Chem. C* **2009**, *113*, 14398.
[61] V. De Cupere, J. Tant, P. Viville, R. Lazzaroni, W. Osikowicz, W. R. Salaneck, Y. H. Geerts, *Langmuir* **2006**, *22*, 7798.
[62] J. G. Son, K. W. Gotrik, C. A. Ross, *ACS Macro Lett.* **2012**, *1*, 1279.
[63] Y. S. Jung, J. B. Chang, E. Verploegen, K. K. Berggren, C. A. Ross, *Nano Lett.* **2010**, *10*, 1000.
[64] C. M. Bates, T. Seshimo, M. J. Maher, W. J. Durand, J. D. Cushen, L. M. Dean, G. Blachut, C. J. Ellison, C. G. Willson, *Science* **2012**, *338*, 775.
[65] T. Nakai, D. Tanaka, M. Hara, S. Nagano, T. Seki, *Langmuir* **2016**, *32*, 909.
[66] Z. Chen, Y.-T. Chan, D. Miyajima, T. Kajitani, A. Kosaka, T. Fukushima, J. M. Lobez, T. Aida, *Nat. Commun.* **2016**, *7*, 13640.
[67] C. C. Kathrein, W. Bai, J. A. Currivan-Incorvia, G. Liontos, K. Ntetsikas, A. Avgeropoulos, A. Boker, L. Tsarkova, C. A. Ross, *Chem. Mater.* **2015**, *27*, 6890.
[68] Semiconductor Industry Association, *2013 International Technology Roadmap for Semiconductors (ITRS)*, SEMATECH, Albany, NY, USA **2013**.

Received: March 30, 2017
Revised: June 1, 2017
Published online: July 24, 2017

